Soft X-Ray Magnetic Circular Dichroism of Vanadium in the Metal–Insulator Two-Phase Region of Paramagnetic V_2O_3 Doped with 1.1% Chromium

Detlef Schmitz,* Carolin Schmitz-Antoniak, Florin Radu, Hanjo Ryll, Chen Luo, Sumanta Bhandary, Silke Biermann, Konrad Siemensmeyer, Heiko Wende, Sergey Ivanov, and Olle Eriksson

V_2O_3 doped with 1.1% Cr is investigated at its isostructural correlation-driven metal–insulator transition near room temperature in its paramagnetic state with X-ray magnetic circular dichroism (XMCD) spectroscopy in external magnetic fields. A relative XMCD amplitude of about 2 permille is observed at the $L_{2,3}$ absorption edges of vanadium as expected for magnetic moment per mass values of the order of $1\,J\,T^{-1}\,kg^{-1}$ from magnetometry and the literature. Across the metal–insulator transition, the vanadium XMCD spectral shape significantly changes. According to atomic multiplet simulations, these changes are due to a changing orbital occupation indicating a changing phase composition. According to estimates used in this study, the dipole moment of the spin density distribution $7\langle T_z \rangle$ in the bulk increases such that the effective vanadium spin moment increases by a few percent with temperature in the two-phase region. Thereby, it partially compensates for the decrease in the relative XMCD amplitude due to a decreasing alignment of the paramagnetic moments. After a few minor temperature cycles, the sample is in a two-phase state in which the XMCD and X-ray linear dichroism spectra hardly depend on the temperature, and the specific electrical resistance is intermediate, showing only a weak sign of the metal–insulator transition.

1. Introduction

The paramagnetic metal–insulator transition in $(V_{1-x}Cr_x)_2O_3$ is generally considered as the prototypical example of a Mott transition, where electronic Coulomb interactions localize the electrons in the vanadium 3d shell. Early on, it has been investigated with electrical resistivity and powder X-ray diffraction measurements. Below 400 K, a first-order transition is found as a function of either Cr concentration, pressure, or temperature. At ambient pressure, this transition amounts to a change of the electrical resistivity by two orders of magnitude. Concomitantly with the metal–insulator transition a structural transition takes place, where the volume changes by about 1.2%, without any change in symmetry.[1,2] The magnetic susceptibility has also been studied over wide

Dr. D. Schmitz
Helmholtz-Zentrum Berlin für Materialien und Energie
Institut für Quantenphänomene in neuen Materialien
Albert-Einstein-Straße 15, D-12489 Berlin, Germany
E-mail: schmitz@helmholtz-berlin.de

Dr. C. Schmitz-Antoniak
Peter Grünberg Institut (PGI-6)
Forschungszentrum Jülich
D-52425 Jülich, Germany

Dr. F. Radu, Dr. H. Ryll
Helmholtz-Zentrum Berlin für Materialien und Energie
Abteilung Materialien für grüne Spintronik
Albert-Einstein-Straße 15, D-12489 Berlin, Germany

Dr. C. Luo
Fakultät für Physik
Technische Universität München
James-Franck-Straße 1, D-85748 Garching b. München, Germany

The ORCID identification number(s) for the author(s) of this article can be found under https://doi.org/10.1002/pssb.201900456.

Dr. S. Bhandary, Prof. S. Biermann
Centre de Physique Théorique, Ecole Polytechnique
CNRS
Institut Polytechnique de Paris
91128 Palaiseau Cedex, France

Dr. K. Siemensmeyer
Helmholtz-Zentrum Berlin für Materialien und Energie
Institut für Quantenphänomene in neuen Materialien
Hahn-Meitner-Platz 1, D-14109 Berlin, Germany

Prof. H. Wende
Fakultät für Physik and Center for Nanointegration Duisburg-Essen (CENIDE)
Universität Duisburg-Essen
Lotharstr. 1, D-47048 Duisburg, Germany

Prof. S. Ivanov
Karpov Institute of Physical Chemistry
3-1/12, Obuha pereulok, Moscow 105064, Russia

Prof. O. Eriksson
Division of Materials Theory
Department of Physics and Astronomy
Uppsala University
Box-516, SE-75120 Uppsala, Sweden

Prof. O. Eriksson
School of Science and Technology
Örebro University
SE-70182 Örebro, Sweden

Cr concentration and temperature ranges. The separation of the total susceptibility into a temperature-independent van Vleck term and a temperature-dependent term yielded Curie–Weiss behavior for the latter. The Curie temperatures and effective magnetic moments were also determined, and the data were found to be consistent with the picture developed on the basis of resistivity and X-ray diffraction investigations.[3]

The spatial distribution of the magnetization induced in the paramagnetic metallic (PM) phase by an external magnetic field has been determined with polarized neutron diffraction. A predominant spherical and a smaller delocalized part of the 3d moment were found using multipole fits.[4]

The orbital occupations have been studied with soft X-ray absorption spectroscopy at the L edges of vanadium varying the angle between the electric field vector of the linearly polarized light and the crystallographic axes along which the orbitals are oriented. By analyzing the X-ray linear dichroism (XLD) spectra, it was found that the problem cannot be mapped onto a single-band Hubbard model because the different phases (antiferromagnetic insulating [AFI], PM, and paramagnetic insulating [PI]) have different orbital occupation ratios. The drastic changes of the band gap and effective bandwidth were also explained by the changes in the orbital occupations[5] as well as the substantial redistribution of electronic states observed with photoemission spectroscopy (PES).[6]

On the theory side, an ab initio description of the paramagnetic metal–insulator transition in V_2O_3[7–10] became possible with the advent of combined density functional dynamical mean field theory (DFT+DMFT) techniques.[11,12] The nature of the Mott–Hubbard transition was found to be strikingly different from the one-band Hubbard model due to orbital degrees of freedom. The transition was shown to be accompanied by a charge transfer from the a_{1g} orbital into the e_g^π states that become half-filled, whereas the a_{1g} states are shifted upwards. The gap opening then takes place between the lower Hubbard band of e_g^π character and the empty a_{1g} states.[8]

In the metallic phase, a prominent quasiparticle peak has been observed experimentally with high-energy high-resolution photoelectron spectroscopy, in agreement with the theoretical predictions.[13] With bulk sensitive hard X-ray photoemission spectroscopy (HAXPES) for metallic V_2O_3, satellites at the low binding energy side of the vanadium 2p core level peaks were found and ascribed to an additional screening channel in the correlated metal phase.[14] A clear correlation between these shakedown satellites and the coherent peak at the Fermi level was demonstrated in the metallic phase with HAXPES.[15]

The coherent electronic excitations have been studied for metallic V_2O_3 with angle-resolved PES. The observed quasiparticle peak at the Fermi energy was regarded as the distinctive spectral feature of a correlated metal. Due to the interplay between wave vector dependence and surface attenuation effects, the quasiparticle peak strongly varies in intensity when the photoelectron emission angle is changed using two different single crystal surfaces. From this angular dependence, a characteristic length scale of at least 4 nm for the attenuation of the coherent electronic excitations has been found[16] in accordance with a theoretical investigation using the Gutzwiller variational approximation.[17]

At the K absorption edge of vanadium, a peak in the pre-edge region was found and ascribed to distorted VO_6 octahedra at the boundary between the coexisting PM and PI phases.[18]

The spatial distribution of the phase separation has been studied with scanning photoemission microscopy (SPEM) using the intensity of the correlation peak at the Fermi level as the contrast mechanism. The formation of spatial regions was revealed, which were described as "metallic clouds within an insulating sky."[19]

In our work, X-ray magnetic circular dichroism (XMCD) was used to investigate the changes of electronic and magnetic properties in course of the PM–PI transition in more detail. The XMCD effect manifests itself in the dependence of the intensities of an X-ray absorption spectrum on the relative orientation between the magnetization of the sample and the polarization vector of the incident circularly polarized radiation. It was first investigated experimentally in 1987.[20] It can be explained in an atomic model for the absorption process, in which an electron is excited from a core state to unoccupied valence states. In the dipole approximation, the transition probabilities for each spin direction depend on the helicity of the exciting radiation due to the dipole selection rules. For solids, according to Fermi's golden rule, the density of empty states must be considered additionally.[21] XMCD is an attractive method as it is element-specific and because two sum rules were developed that relate the orbital moment[22] and the effective spin moment[23] to areas under the XMCD and the absorption spectrum. The effective spin moment is the sum of the pure spin moment and the dipole moment of the spin density distribution. The second term contains the expectation value of the dipole operator $\langle T_z \rangle$, and it can be expressed as a product between the spin moment and the charge quadrupolar tensor.

The $\langle T_z \rangle$ term has turned out to be a powerful monitor for the Verwey transition in magnetite.[24] The Verwey transition is a metal–insulator transition as well, but connected to a structural change from cubic to monoclinic upon cooling. That is, the crystal structure changes from a symmetry where all components of $\langle T_\alpha \rangle$ vanish to a symmetry where the components no longer vanish, whereas the pure spin moment does not abruptly change at the transition.

In this study, XMCD spectroscopy is applied to a metal–insulator transition that is not accompanied by an abrupt change of crystal structure symmetry[1] but which is correlation-driven and related to the electronic structure, i.e., the Mott–Hubbard transition from the PM to the PI state in $(V_{1-x}Cr_x)_2O_3$ with a Cr content x of 1.1%. The small relative XMCD amplitude of about 2 permille is explained by the small magnetization values in the temperature regime of the transition. Changes in spectral shape and intensity are discussed in terms of orbital occupation related to the phase transition by comparison with charge transfer multiplet simulations using the CTM4XAS program package.[25] Pure thermal effects, i.e., the incomplete alignment of paramagnetic moments by the external magnetic field and the thermally induced occupation of electronic states, are discussed and the influence of $\langle T_z \rangle$ is estimated. In addition, we show that after a few temperature cycles the sample is in a PM–PI two-phase state in which the relative XMCD amplitude, the electrical resistance, and the relative XLD amplitude hardly depend on the sample temperature.

2. Results and Discussion

The PM–PI transition temperature of $(V_{1-x}Cr_x)_2O_3$ strongly depends on the Cr content x as schematically shown in the phase diagram (**Figure 1**) adapted from Figure 9 in the study by McWhan and Remeika.[2] For the present Cr concentration of 1.1%, it is between 275 and 300 K on heating and below 260 K on cooling according to infrared spectroscopy and surface-sensitive SPEM[19] using a sample from the same batch as ours. This has been verified for the present sample with electrical resistance measurements of a "pristine" sample piece where the metal–insulator transition is clearly visible (Figure S2, Supporting Information). XMCD spectra in the PM–PI two-phase region have to be taken at these elevated temperatures where the aligned paramagnetic moments are reduced by about two orders of magnitude compared with low temperatures of a few Kelvin as described by the Brillouin function (**Figure 2**). Accordingly, the expected relative XMCD amplitude at the vanadium $L_{2,3}$ edges is only a few permille, corresponding to a magnetic moment of the order of $10^{-2}\,\mu_B$ per V ion as estimated by comparing with the calculated XMCD spectra, which is in reasonable agreement with vibrating sample magnetometry (VSM) data.

XLD and corresponding X-ray absorption near edge structure (XANES) spectra at 280 K are shown in **Figure 3**a. The measurements (red lines) were performed using horizontal (H) and vertical (V) linear polarization of the undulator radiation with the electric field vector parallel and perpendicular to the hexagonal **c** axis of the crystal lattice, respectively. XLD spectra (H–V) with a relative amplitude of about 10% were observed in accordance with the study by Park et al.[5] XMCD and corresponding XANES spectra at 260 K are shown in Figure 3b. The relative XMCD amplitude is only about 2 permille due to the elevated temperature as discussed earlier, and in accordance with magnetic moment per mass values of the order of $1\,J\,T^{-1}\,kg^{-1}$ from VSM and the literature. It is close to the detection limit of

Figure 2. Brillouin function for V^{3+} ($3d^2$) with total angular momentum $J = 2$, g-factor $g = 2/3$, and magnetic flux density $\mu_0H = 8\,T$. Since the PM–PI two-phase region exists at temperatures around 275 K (dashed line), the aligned paramagnetic moments are reduced by about two orders of magnitude compared with low temperatures of a few Kelvin.

the XMCD method and requires a stable experimental setup and a careful data analysis.

Nevertheless, all main features of the measured vanadium spectra are reproduced in the CTM4XAS simulations (black lines). In the simulations, the rhombohedral symmetry of the crystal structure of V_2O_3 is expressed with the parameters $10Dq$ and Dt, which describe the $t_{2g} - e_g$ crystal field splitting and the additional trigonal distortion which splits the t_{2g} orbitals into a nondegenerate a_{1g} and doubly degenerate orbitals. As noted by Park et al.,[5] "the a_{1g} orbital has lobes directed along the **c** vector of the hexagonal basis, whereas the e_g lobes are more within the (**a**,**b**) basal plane." Therefore, XLD spectra, measured in the geometry described earlier, are sensitive to the orbital occupation ratios, which are known to change in course of the phase transition.[9] Here, the measured spectra are best described with a simulated spectrum using a $10Dq$ value of $2\,eV$ and consisting of 40% of a spectrum with a positive Dt of $0.05\,eV$ (blue line) and 60% of a spectrum with a negative Dt of $-0.075\,eV$ (magenta line). Negative and positive values of Dt are used to model occupation of different orbitals. In the simulations, the same values of the crystal field parameters were used for the XLD and XMCD spectra, as well as for the corresponding XANES spectra. This consistency indicates that the present system can be simulated reasonably well within the CTM4XAS framework.[25]

Moreover, the CTM4XAS simulations have the advantage that the effect of a changing phase composition and purely temperature-induced changes can be separated. This is shown in **Figure 4**. Changing the ratio of the weighting factors from 4:6 to 6:4 (in accordance with the trend of the orbital occupation ratios in the study by Park et al.[5]) slightly decreases the XMCD amplitude at the low-energy side of the L_3 line (below 515 eV) and significantly increases the XMCD amplitude at the high-energy side of the L_3 line and at the L_2 line (Figure 4, top panel). In contrast, changing the occupation by varying the temperature from 260 to 300 K for a fixed ratio of 4:6 significantly decreases the XMCD amplitude over the whole spectral range (Figure 4, bottom panel). That is, both effects add up at the
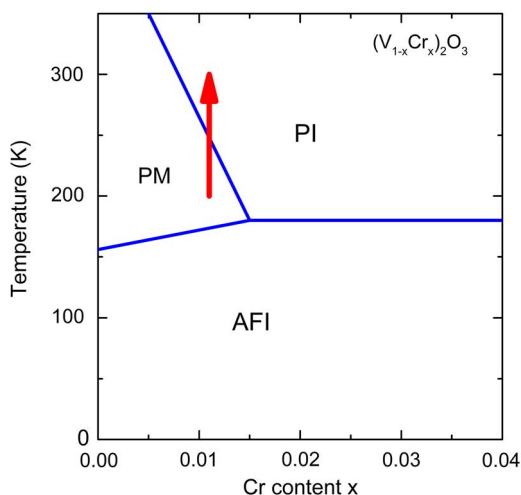

Figure 1. Phase diagram of $(V_{1-x}Cr_x)_2O_3$ including the AFI, the PM and the PI phases. Adapted with permission.[2] Copyright 2019, American Physical Society. The red arrow indicates that in the present experiments, the PM–PI phase composition was changed by increasing the temperature.
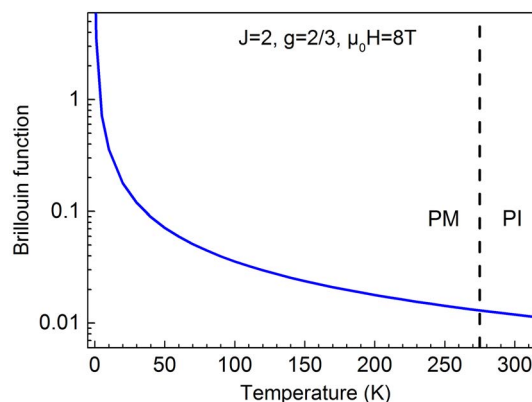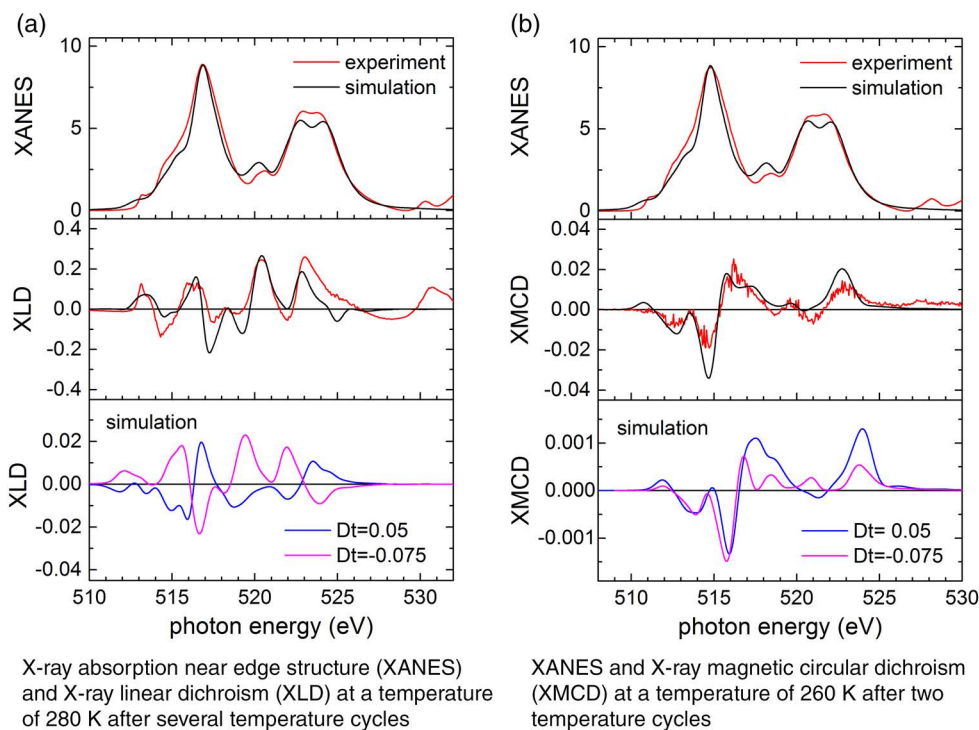
ADVANCED
SCIENCE NEWS
www.advancedsciencenews.com

physica
status
solidi
pss b
www.pss-b.com

(a) X-ray absorption near edge structure (XANES) and X-ray linear dichroism (XLD) at a temperature of 280 K after several temperature cycles

(b) XANES and X-ray magnetic circular dichroism (XMCD) at a temperature of 260 K after two temperature cycles

Figure 3. a) XLD, b) XMCD, and corresponding XANES spectra at the vanadium $L_{2,3}$ edges in the PM–PI two-phase region of $(V_{1-x}Cr_x)_2O_3$ with $x = 0.011$. The measurements (red lines) are compared with CTM4XAS simulations (black lines). The simulated XLD and XMCD spectra each consist of two spectra with $Dt = 0.05$ (blue lines) and $Dt = -0.075$ (magenta lines) weighted with a ratio of 4:6. For these XLD, XMCD, and corresponding XANES spectra, the same values of the crystal field parameters were used.
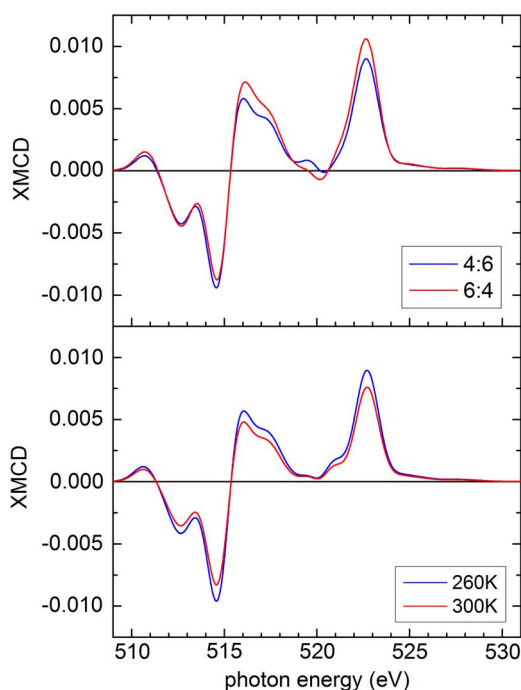

Figure 4. Simulated XMCD spectra for different phase compositions at a fixed temperature of 260 K (top panel) and at different temperatures for a fixed weighting factor ratio of 4:6 (bottom panel).

low-energy side of the L_3 line, whereas they partially compensate for each other at photon energies above 515 eV. In the following sections, the resulting spectral changes are compared with the measurements.

In **Figure 5**, top panel, two XMCD spectra measured at 260 (blue line) and 320 (red line) K after heating from 220 K, following the temperatures for the surface-sensitive SPEM measurements in the study by Lupi et al.,[19] are shown as an example. With increasing temperature, a significant change of the spectral shape is observed, which mainly consists of a decreasing intensity at the low-energy side of the L_3 line (below 515 eV), an increasing intensity at the high-energy side of the L_3 line (above 515 eV), a decrease in the small peak at 519.5 eV, and an increasing intensity around 521 eV. Remarkably, all four changes of the measured spectral shape are also present in the simulation (Figure 5, bottom panel), and thus can be explained with a combination of changing phase composition and temperature. To demonstrate that the aforementioned changes of the measured spectral shape are systematically developing with temperature, the normalized XMCD spectra measured after the first cleaving are shown in Figure S4, Supporting Information.

The dependence of the relative XMCD amplitude on the sample temperature is discussed in the following sections. From the Brillouin function (Figure 2), it is expected that the relative XMCD amplitude decreases by about 19% from 260 to 320 K. This is partly compensated for by another effect: XMCD is sensitive to the effective spin moment, which consists
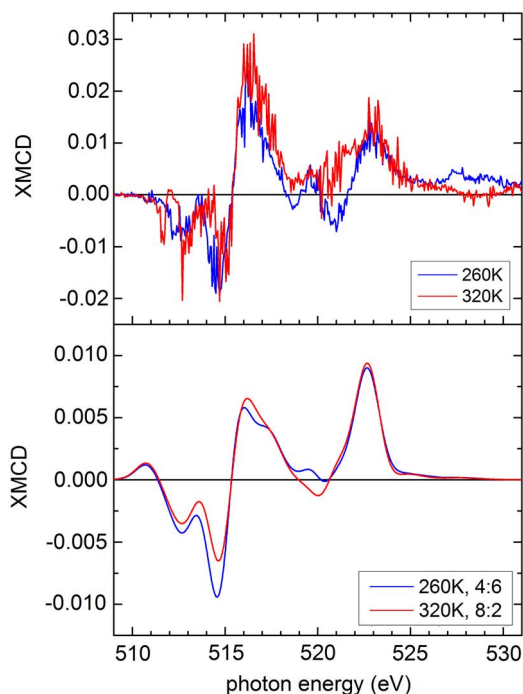
Figure 5. Comparison of measured (top panel) and simulated (bottom panel) XMCD spectra at 260 K (blue lines) and 320 K (red lines) in the PM–PI two-phase region. In the simulations weighting factor ratios of 4:6 at 260 K and 8:2 at 320 K were used.

Figure 6. Estimated local spin moment plus the dipole moment of the spin density distribution $7\langle T_z\rangle$ of vanadium versus temperature while heating (red squares) and cooling (blue circles).

of the spin moment plus the dipole moment of the spin density distribution $7\langle T_z\rangle$.[23] Therefore, a change of $7\langle T_z\rangle$ also has to be considered in the analysis of the XMCD amplitude with temperature. Here, the local effective spin moment of vanadium is estimated as a function of temperature by taking the density matrix obtained in the local density approximation plus dynamical mean field theory (LDA+DMFT) study by Poteryaev et al.,[9] expressing the density matrix in cubic harmonics, considering relatively weak spin–orbit coupling, and considering the geometry of the XMCD experiment as well as the phase percentages for heating and cooling from XRD experiments in the study by McWhan and Remeika.[2] As shown in **Figure 6**, it linearly increases from 220 to 340 K for heating and decreases with a rounded shape for cooling, thereby showing a hysteretic behavior. It is to be noted that the values in Figure 6 are for the local moments, having random orientations in the paramagnetic phase and being only partly aligned by the external magnetic field applied in the experiments. However, the relative increase by 5% from 200 to 340 K is not affected by the partial alignment. That is, $7\langle T_z\rangle$ tends to increase the XMCD amplitude with temperature, thereby partly compensating for the decreasing alignment of the paramagnetic magnetic moments according to the Brillouin function. Unfortunately, these two competing effects cannot be quantitatively separated in this experiment in view of the tiny relative XMCD amplitudes and the associated experimental uncertainties.

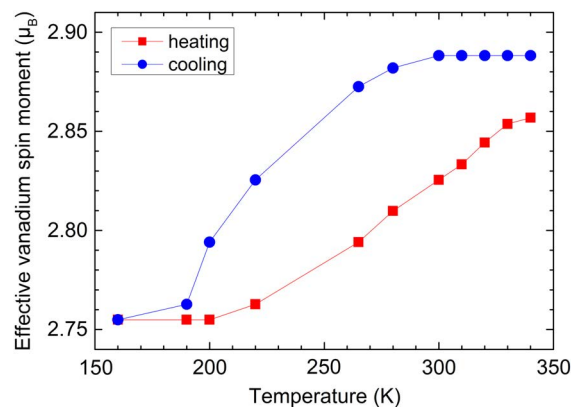The XMCD spectra shown in Figure 5, top panel, were measured after the first cleave and during the first two temperature cycles, i.e., cooling to 220 K and heating stepwise to the desired temperatures. During all sample cooling procedures, special care was taken not to cool the sample below 200 K to safely stay above the structurally destructive transition from the PM to the AFI phase at about 170 K for decreasing temperature.[2] The highest sample temperature during the dichroism measurements was limited by the sample cryostat and set to 320 K in the first and between 300 and 315 K in later temperature cycles as described in the Supporting Information. In other words, the temperature cycles were "minor," i.e., the temperature scanning direction was reversed several times before reaching the pure PM or PI phases. In this way, the sample reached a state in which the XMCD amplitude and its change with temperature significantly decreased with respect to the first two temperature cycles. The relative XMCD amplitudes during the third and fourth temperature cycles decreased to about two-thirds relative to the ones from the first and second temperature cycles. Consequently, during the second beamtime, it was not straightforward to measure relative XMCD amplitudes at more temperatures that fit to the ones from the first beamtime.

Cleaving the sample a second time recovered neither the initial XMCD amplitude nor its strong temperature dependence as shown in the Supporting Information. In contrast, in this way, further oxidation at the sample surface can be excluded as a reason for the overall XMCD decrease. A significant Cr concentration gradient in the samples can also be excluded as a reason because the Cr concentration measured at ten different positions of the ingot ranged from 0.985% to 1.162% (see Supporting Information), corresponding to a transition temperature interval of only about 15 K. Moreover, the cap piece of the second cleaving of the single crystal was retrieved from the preparation chamber and used for resistance measurements shown in Figure S6, Supporting Information. The specific resistance of the cap piece was about 0.6 Ω cm, which is between the values for the PM and PI phases (0.1 and 2 Ω cm, respectively) of a sample with 1% Cr given in Figure 8 of ref. [2], and it changed by only a few percent around 275 K, whereas the change in ref. [2] was more than one order of magnitude. Such a behavior was already observed and analyzed by Honig et al.:[26] "By heating or cooling samples that had repeatedly been cycled through the high-temperature

range, the anomaly in this region could be almost totally suppressed."

In addition, the temperature-cycled state of the present sample was characterized with XLD measurements after cleaving the sample a third time. It was found that the XLD and corresponding XANES spectra hardly changed with temperature from 240 via 280 to 310 K as shown in Figure S7, Supporting Information, indicating that the phase composition hardly changed. Therefore, after a few "minor" temperature cycles, the sample was finally in a PM–PI two-phase state showing only weak traces of the metal–insulator transition.

3. Conclusions

In summary, the following results were found: 1) The relative XMCD amplitude at the vanadium $L_{2,3}$ absorption edges is only a few permille in an external magnetic field of 8 T due to the elevated temperatures (around 275 K) of the PM–PI two-phase region. This small value is in accordance with the magnetic moment per mass values of the order of $1 \, J \, T^{-1} \, kg^{-1}$ measured with VSM and values from the literature. 2) In the PM–PI transition region, the XMCD spectral shape changes with temperature. According to CTM4XAS simulations, these changes are due to a combination of a changing phase composition and pure temperature effects. 3) The main features in the XANES, XLD, and XMCD spectra are reproduced in the CTM4XAS simulations using the same values of the crystal field parameters, indicating that the present system can be simulated reasonably well within the CTM4XAS framework. 4) In the PM–PI two-phase region, the increase in the effective spin moment due to the changing spin-dipole moment $7\langle T_z \rangle$ as a function of temperature is estimated to be only 5%. Thereby, it partially compensates for the decrease in the relative XMCD amplitude due to a decreasing alignment of the paramagnetic moments with increasing temperature. 5) After a few "minor" temperature cycles, the sample is in a PM–PI two-phase state in which the relative XMCD amplitude and its change with temperature are significantly reduced, the electrical resistance is intermediate, showing only a weak local maximum around the PM–PI transition temperature, and the relative XLD amplitude hardly depends on the sample temperature.

4. Experimental Section

The $(V_{0.989}Cr_{0.011})_2O_3$ single crystal was grown with the skull-melting technique under carefully controlled conditions as described in the study by Metcalf and Honig.[27] The composition and the lattice parameters were checked with energy dispersive X-ray spectroscopy, inductively coupled plasma mass spectrometry, and high-resolution X-ray single crystal diffraction, respectively. The ingot was aligned with Laue diffraction and cut to rectangular bars with a diamond wire saw at the CoreLab Quantum Materials[28] of the Helmholtz-Zentrum Berlin für Materialen und Energie (HZB) and finally cleaved in ultrahigh vacuum in situ before the soft X-ray dichroism measurements at two different beamlines of the electron storage ring BESSY II of HZB. For the XMCD measurements, the single crystal was mounted such that the (-102) direction was parallel to the direction of the incident photon beam and to the magnetic field axis as shown in Figure S1, Supporting Information. The XMCD measurements were performed with the VEKMAG endstation[29] at the dipole beamline PM2 reversing several times the magnetic field between +8

and −8 T between complete photon energy scans for each helicity of the elliptically polarized dipole radiation with a circular polarization degree of 80%. For the XLD measurements, the single crystal was mounted such that the (001) axis, i.e., the hexagonal c axis, was parallel to the electric field vector **E** of the horizontal linear polarization and the (110) plane, i.e., the (**a**,**b**) basal plane, parallel to the **E** vector of the vertical linear polarization of the incident photon beam as shown in Figure S1, Supporting Information. The XLD measurements were performed with the high-field endstation at the elliptical undulator beamline UE46-PGM1[30] using horizontal and vertical linear polarization of the undulator radiation. More details about the sample preparation, magnetization, and resistance measurements as well as the experimental setups are presented in the Supporting Information.

Conflict of Interest

The authors declare no conflict of interest.

[1] D. B. McWhan, T. M. Rice, J. P. Remeika, *Phys. Rev. Lett.* **1969**, *23*, 1384.

[2] D. B. McWhan, J. P. Remeika, *Phys. Rev. B* **1970**, *2*, 3734.

[3] A. Menth, J. P. Remeika, *Phys. Rev. B* **1970**, *2*, 3756.

[4] P. J. Brown, M. M. R. Costa, K. R. A. Ziebeck, *J. Phys.: Condens. Matter* **1998**, *10*, 9581.

[5] J.-H. Park, L. H. Tjeng, A. Tanaka, J. W. Allen, C. T. Chen, P. Metcalf, J. M. Honig, F. M. F. de Groot, G. A. Sawatzky, *Phys. Rev. B* **2000**, *61*, 11506.

[6] K. E. Smith, V. E. Henrich, *Phys. Rev. B* **1994**, *50*, 1382.

[7] P. Hansmann, A. Toschi, G. Sangiovanni, T. Saha-Dasgupta, S. Lupi, M. Marsi, K. Held, *Phys. Status Solidi B* **2013**, *250*, 1251.

[8] G. Keller, K. Held, V. Eyert, D. Vollhardt, V. I. Anisimov, *Phys. Rev. B* **2004**, *70*, 205116.

[9] A. I. Poteryaev, J. M. Tomczak, S. Biermann, A. Georges, A. I. Lichtenstein, A. N. Rubtsov, T. Saha-Dasgupta, O. K. Andersen, *Phys. Rev. B* **2007**, *76*, 085127.

[10] J. M. Tomczak, S. Biermann, *J. Phys.: Condens. Matter* **2009**, *21*, 064209.

[11] A. I. Lichtenstein, M. I. Katsnelson, *Phys. Rev. B* **1998**, *57*, 6884.

[12] V. I. Anisimov, A. I. Poteryaev, M. A. Korotin, A. O. Anokhin, G. Kotliar, *J. Phys.: Condens. Matter* **1997**, *9*, 7359.

[13] S.-K. Mo, J. D. Denlinger, H.-D. Kim, J.-H. Park, J. W. Allen, A. Sekiyama, A. Yamasaki, K. Kadono, S. Suga, Y. Saitoh, T. Muro, P. Metcalf, G. Keller, K. Held, V. Eyert, V. I. Anisimov, D. Vollhardt, *Phys. Rev. Lett.* **2003**, *90*, 186403.

[14] N. Kamakura, M. Taguchi, K. Yamamoto, K. Horiba, A. Chainani, Y. Takata, E. Ikenaga, H. Namatame, M. Taniguchi, M. Awaji, A. Takeuchi, K. Tamasaku, Y. Nishino, D. Miwa, T. Ishikawa, Y. Ueda, K. Kobayashi, S. Shin, *J. Electron Spectrosc. Relat. Phenom.* **2005**, *144–147*, 841.

[15] G. Panaccione, M. Sacchi, P. Torelli, F. Offi, G. Cautero, R. Sergo, A. Fondacaro, C. Henriquet, S. Huotari, G. Monaco, L. Paolasini, *Phys. Rev. Lett.* **2006**, *97*, 116401.

[16] F. Rodolakis, B. Mansart, E. Papalazarou, S. Gorovikov, P. Vilmercati, L. Petaccia, A. Goldoni, J. P. Rueff, S. Lupi, P. Metcalf, M. Marsi, *Phys. Rev. Lett.* **2009**, *102*, 066805.

[17] G. Borghi, M. Fabrizio, E. Tosatti, *Phys. Rev. Lett.* **2009**, *102*, 066806.

[18] D. M. Pease, A. I. Frenkel, V. Krayzman, T. Huang, P. Shanthakumar, J. I. Budnick, P. Metcalf, F. A. Chudnovsky, E. A. Stern, *Phys. Rev. B* **2011**, *83*, 085105.

[19] S. Lupi, L. Baldassarre, B. Mansart, A. Perucchi, A. Barinov, P. Dudin, E. Papalazarou, F. Rodolakis, J.-P. Rueff, J.-P. Iti, S. Ravy, D. Nicoletti, P. Postorino, P. Hansmann, N. Parragh, A. Toschi, T. Saha-Dasgupta, O. K. Andersen, G. Sangiovanni, K. Held, M. Marsi, *Nat. Commun.* **2010**, *1*, 105.

[20] G. Schütz, W. Wagner, W. Wilhelm, P. Kienle, R. Zeller, R. Frahm, G. Materlik, *Phys. Rev. Lett.* **1987**, *58*, 737.

[21] J. Stöhr, *NEXAFS Spectroscopy*, Springer Series in Surface Sciences, Vol. *25*, Springer, Berlin Heidelberg, Germany **1992**.

[22] B. T. Thole, P. Carra, F. Sette, G. van der Laan, *Phys. Rev. Lett.* **1992**, *68*, 1943.

[23] P. Carra, B. T. Thole, M. Altarelli, X. Wang, *Phys. Rev. Lett.* **1993**, *70*, 694.

[24] D. Schmitz, C. Schmitz-Antoniak, A. Warland, M. Darbandi, S. Haldar, S. Bhandary, O. Eriksson, B. Sanyal, H. Wende, *Sci. Rep.* **2014**, *4*, 5760.

[25] E. Stavitski, F. M. F. de Groot, *Micron* **2010**, *41*, 687.

[26] J. M. Honig, G. V. Chandrashekhar, A. P. B. Sinha, *Phys. Rev. Lett.* **1974**, *32*, 13.

[27] P. A. Metcalf, J. M. Honig, *Curr. Top. Cryst. Growth Res.* **1995**, *2*, 445.

[28] www.helmholtz-berlin.de/quellen/corelabs/quantum-materials (accessed: October 2019).

[29] T. Noll, F. Radu, *Proc. of MEDSI 2016*, Joint Accelerator Conferences Website, Geneva, Switzerland **2017**, p. 370.

[30] U. Englisch, H. Rossner, H. Maletta, J. Bahrdt, S. Sasaki, F. Senf, K. J. S. Sawhney, W. Gudat, *Nucl. Instrum. Methods Phys. Res. Sect. A* **2001**, *467–468*, 541.